

## **$N$ to $\Delta$ electromagnetic and axial form factors in full QCD**

C. Alexandrou

*Department of Physics, University of Cyprus, P.O. Box 20537, 1678, Nicosia, Cyprus*  
*E-mail: alexand@ucy.ac.cy, www.ucy.ac.cy*

Lattice results on the  $N$  to  $\Delta$  electromagnetic, axial-vector and pseudoscalar form factors are evaluated using dynamical staggered sea quarks and domain wall valence quarks for pion masses in the range of 580-350 MeV, as well as, dynamical and quenched Wilson fermions for similar pion masses.

*Keywords:* Lattice QCD, Form factors, Nucleon Resonances

### **1. Introduction**

State-of-the-art lattice QCD calculations can yield model independent results on  $N$  to  $\Delta$  transition form factors, thereby providing direct comparison with experiment. One such example is the  $N$  to  $\Delta$  quadrupole form factors that have been accurately measured in a series of recent experiments at low [1,2] and high momentum transfers [3]. They encode information on the deformation of the nucleon and  $\Delta$ . We present results on these  $N$  to  $\Delta$  electromagnetic form factors, as well as on the dominant axial-vector  $N$  to  $\Delta$  transition form factors  $C_5^A(q^2)$  and  $C_6^A(q^2)$ . Experiments using electroproduction of the  $\Delta$  resonance are in the progress [4] to measure the parity violating asymmetry in  $N$  to  $\Delta$ , which, to leading order, is connected to  $C_5^A(q^2)$ . Evaluation of the pseudoscalar  $\pi N \Delta$  form factor,  $G_{\pi N \Delta}(q^2)$ , follows once the  $N$  to  $\Delta$  sequential propagators are computed. In addition, we evaluate the nucleon axial-vector form factors and the  $\pi N N$  form factor,  $G_{\pi N N}(q^2)$ . Having both the nucleon and the  $N$  to  $\Delta$  form factors allows us to discuss ratios of form factors that are expected to show weaker quark mass dependence and be less sensitive to other lattice artifacts. Furthermore, knowledge of the axial-vector form factors and the  $\pi N N$  and  $\pi N \Delta$  form factors allows us to check the Goldberger-Treiman relations.

The light quark regime is studied in two ways: Besides using configurations with two degenerate flavors of dynamical Wilson fermions we use a hybrid combination of domain wall valence quarks, which have chiral symmetry on the lattice, and MILC configurations generated with three flavors of staggered sea quarks using the Asqtad improved action [5].

### **2. Lattice Techniques**

Observables in lattice QCD are given by the vacuum expectation value of gauge invariant operators in Euclidean time:

$$\langle \Omega | \hat{O} | \Omega \rangle = \frac{1}{Z} \int d[U] d[\bar{\psi}] d[\psi] O[U, \bar{\psi}, \psi] e^{-S_g[U] - S_F[U, \bar{\psi}, \psi]} \quad (1)$$

Integrating over the fermionic degrees of freedom we obtain

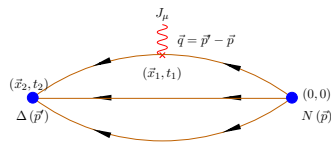
$$< \Omega | \hat{O} | \Omega > = \frac{1}{Z} \int d[U] \det(D[U]) O[U, D^{-1}[U]] e^{-S_g[U]} \quad (2)$$

where  $D_{jn}^{-1}[U]$  substitutes each appearance of  $-\bar{\psi}_n \psi_j$  in the operator and describes valence quarks whereas  $\det(D[U])$  corresponds to sea quarks. The path integral over the gauge fields is done numerically by stochastically generating a representative ensemble of gauge configurations according to the probability  $P[U] = \frac{1}{Z} \exp \{-S_g[U] + \ln(\det(D[U]))\}$ . (3)

In this work, besides Wilson fermions for the sea and valence quarks, we use staggered sea quarks ( $\det(D_{\text{staggered}}[U])$ ) and domain wall valence fermions ( $D_{\text{DW}}^{-1}[U]$ ). The expectation values are obtained by summing over the  $U$ -ensemble:  $< \Omega | \hat{O} | \Omega > = \lim_{N \rightarrow \infty} \frac{1}{N} \sum_{k=1}^N O[U^k, D^{-1}[U^k]]$ .

The evaluation of form factors involves taking numerically the Fourier transform of two- and three-point functions with respect to momentum transfer which, on a finite box of spatial length  $L$ , takes discrete values in units of  $2\pi/L$ . For large values of momentum transfer the results become noisy and therefore we are limited up to  $Q^2 \equiv -q^2 \sim 2 \text{ GeV}^2$ . To ensure that finite volume effects are kept small we take box sizes such that  $Lm_\pi \gtrsim 4.5$ , where  $m_\pi$  is the pion mass<sup>a</sup>. In addition, discretization errors due to the finite lattice spacing  $a$  must be checked. Wilson fermions have  $\mathcal{O}(a)$  discretization errors and staggered fermions with Asqtad action and domain wall fermions (hybrid approach) have  $\mathcal{O}(a^2)$  errors. Therefore agreement between results in these two approaches provides an indication that cut-off effects are under control. Finally, we use larger bare u- and d-quark masses than physical and extrapolation to the chiral limit must be considered.

Form factors are extracted from three-point functions,  $G^{\Delta JN}(t_2, t_1; \mathbf{q}) = < \Omega | \sum_{\mathbf{x}_1, \mathbf{x}_2} e^{i\mathbf{q} \cdot \mathbf{x}_1} \hat{T} \hat{J}_h(\mathbf{x}_2, t_2) \hat{J}(\mathbf{x}_1, t_1) \hat{J}_h^\dagger(0) | \Omega >$ , shown in the diagram below:



Interpolating fields for N and  $\Delta$  are:

$$\begin{aligned} J^p(x) &= \epsilon^{abc} [u^{Ta}(x) C \gamma_5 d^b(x)] u^c(x), \\ J_\sigma^{\Delta+}(x) &= \frac{1}{\sqrt{3}} \epsilon^{abc} \{ 2[u^{Ta}(x) C \gamma_\sigma d^b(x)] u^c(x) \\ &\quad + [u^{Ta}(x) C \gamma_\sigma u^b(x)] d^c(x) \} \end{aligned}$$

In all cases we apply Gaussian smearing at the source and sink. In the

<sup>a</sup>One exception is in the case of dynamical Wilson fermions at the smallest pion mass for which  $Lm_\pi = 3.6$  as marked in the Table.

case of unquenched Wilson fermions HYP-smearing is applied to the gauge links used in the Gaussian smearing of the source and sink. In the case of domain wall fermions we use HYP-smeared MILC configurations in all computations. We carry out sequential inversions by fixing the quantum numbers at the sink and source, which means that the sink time  $t_2$  is fixed, whereas the insertion time  $t_1$  can vary and any operator can be inserted at  $t_1$ . In this work we consider the vector current,  $j_\mu^a = \bar{\psi}\gamma_\mu \frac{\tau^a}{2}\psi$ , the axial-vector current,  $A_\mu^a = \bar{\psi}\gamma_\mu\gamma_5 \frac{\tau^a}{2}\psi$  and the pseudoscalar current,  $P^a = \bar{\psi}i\gamma_5 \frac{\tau^a}{2}\psi$ , where  $\tau^a$  are Pauli matrices acting in flavor space. All  $\vec{x}_1$  and  $\vec{x}_2$  are summed over and we vary  $t_1$  in search for a plateau. The exponential time dependence and unknown overlaps of the interpolating fields with the physical states cancel by dividing the three-point function with appropriate combinations of two-point functions [6].

The lattice parameters that we use are given in the Table.

Wilson fermions						
number of confs	$\kappa$	$m_\pi$ (GeV)		$m_N$ (GeV)		
Quenched $32^3 \times 64$ , $\beta = 6.0$ , $a^{-1} = 2.14(6)$ GeV ( $a = 0.09$ fm) from nucleon mass at chiral limit						
200	0.1554	0.563(4)		1.267(11)		
200	0.1558	0.490(4)		1.190(13)		
200	0.1562	0.411(4)		1.109(13)		
	$\kappa_c = 0.1571$	0.		0.938(9)		
Unquenched [7] $24^3 \times 40$ , $\beta = 5.6$ , $a^{-1} = 2.56(10)$ GeV ( $a = 0.08$ fm)						
185	0.1575	0.691(8)		1.485(18)		
157	0.1580	0.509(8)		1.280(26)		
Unquenched [8] $24^3 \times 32$ , $\beta = 5.6$ , $a^{-1} = 2.56(10)$ GeV						
200	0.15825	$0.384(8) \leftarrow Lm_\pi = 3.6$		1.083(18)		
	$\kappa_c = 0.1585$	0.		0.938(33)		

Hybrid scheme $a^{-1} = 1.58$ GeV ( $a = 0.125$ fm) from MILC collaboration						
number of confs	Volume	$(am_{u,d})^{\text{sea}}$	$(am_s)^{\text{sea}}$	$(am_q)^{DW}$	$m_\pi^{DW}$ (GeV)	$m_N$ (GeV)
150	$20^3 \times 64$	0.03	0.05	0.0478	0.589(2)	1.392(9)
198	$20^3 \times 64$	0.02	0.05	0.0313	0.501(4)	1.255(19)
100	$20^3 \times 64$	0.01	0.05	0.0138	0.362(5)	1.138(25)
150(300 for CMR)	$28^3 \times 64$	0.01	0.05	0.0138	0.354(2)	1.210(24)

### 3. $N$ to $\Delta$ electromagnetic form factors

The  $N$  to  $\Delta$  matrix element of the electromagnetic current can be decomposed into a dominant magnetic dipole,  $G_{M1}$ , and two suppressed electric and Coulomb quadrupole form factors,  $G_{E2}$  and  $G_{C2}$ . A non-zero  $G_{E2}$  and  $G_{C2}$  signal a deformation in the nucleon and/or  $\Delta$ . Precise experimental data on the quadrupole to dipole ratios,  $R_{EM}(\text{EMR}) = -\frac{G_{E2}(q^2)}{G_{M1}(q^2)}$ , and  $R_{SM}(\text{CMR}) = -\frac{|\vec{q}|}{2m_\Delta} \frac{G_{C2}(q^2)}{G_{M1}(q^2)}$ , suggest deformation of the nucleon/ $\Delta$  [9].

In Fig. 1 we show the EMR and CMR ratios for the smallest pion mass

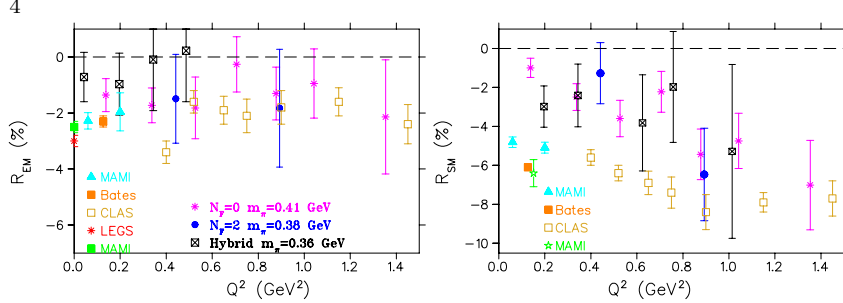


Fig. 1. The EMR (left) and CMR (right) for the lightest pion mass in our three type of simulations.

in the quenched case, for two dynamical flavors of Wilson fermions and in the hybrid approach. For the first time in full QCD, we achieve good enough accuracy to exclude a zero value for these ratios. Furthermore, at low  $Q^2$ , unquenched results become more negative bringing lattice results closer to experiment and showing the importance of the pion cloud effects at small  $Q^2$ .

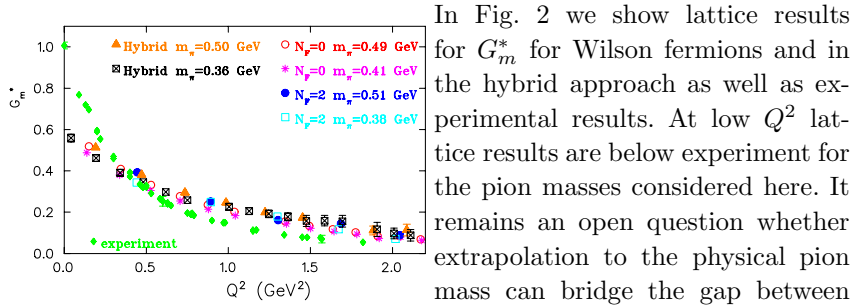


Fig. 2. Magnetic dipole form factor  $G_m^*$ , in the Ash parameterization:  $G_m^* = \frac{1}{\sqrt{1 + \frac{Q^2}{(m_N + m_\Delta)^2}}} G_{M1}$ .

#### 4. Nucleon and N to $\Delta$ axial-vector form factors

In the case of Wilson fermions, besides N to  $\Delta$  we also calculate the nucleon axial-vector form factors. The LHP collaboration [10] has evaluated these form factors in the hybrid approach with the same parameters as those used in our N to  $\Delta$  study and therefore, in this case, we use their results to compare. The nucleon axial- vector form factors  $G_A$  and  $G_p$  are given by

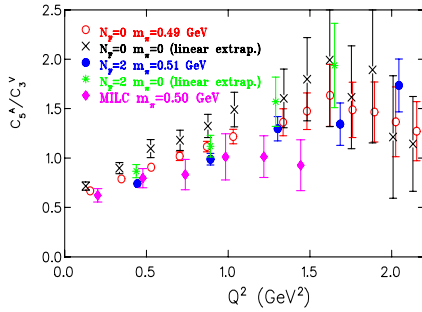
$$\langle N(p') | A_\mu^3 | N(p) \rangle = i \sqrt{\frac{m_N^2}{E_N(\mathbf{p}') E_N(\mathbf{p})}} \bar{u}(p') \left[ G_A(q^2) \gamma_\mu \gamma_5 + \frac{q_\mu \gamma_5}{2m_N} G_p(q^2) \right] \frac{\tau^3}{2} u(p) \quad (4)$$

Since the final state is no longer the  $\Delta$  a new set of sequential inversions is needed. The decomposition of the N to  $\Delta$  matrix element of the axial-vector

current can be written in terms of four transition form factors [11]:

$$\begin{aligned} \langle \Delta(p', s') | A_\mu^3 | N(p, s) \rangle = & i \sqrt{\frac{2}{3}} \sqrt{\frac{m_N m_\Delta}{E_\Delta(\mathbf{p}') E_N(\mathbf{p})}} \bar{u}_{\Delta+}^\lambda(p', s') \left[ C_5^A(q^2) g_{\lambda\mu} \right. \\ & \left. + \frac{C_6^A(q^2)}{m_N^2} q_\lambda q_\mu + \left( \frac{C_3^A(q^2)}{m_N} \gamma^\nu + \frac{C_4^A(q^2)}{m_N^2} p'^\nu \right) (g_{\lambda\mu} g_{\rho\nu} - g_{\lambda\rho} g_{\mu\nu}) q^\rho \right] u_P(p, s) \end{aligned} \quad (5)$$

Under the assumptions that  $C_3^A \sim 0$  and  $C_4^A \ll C_5^A$  the parity violating asymmetry is proportional to the ratio  $C_5^A/C_3^V$  [12], where  $C_3^V$  can be obtained from the electromagnetic N to  $\Delta$  transition.



As shown in Fig. 3, the asymmetry is non-zero when  $Q^2 = 0$  [6], increases with  $Q^2$  up to about  $Q^2 \sim 1.5 \text{ GeV}^2$  and shows small unquenching effects for this range of quark masses. Given this weak quark mass dependence, the results can be taken as a prediction for the ratio to be measured by the G0 collaboration [4].

Fig. 3. Parity violating asymmetry.

#### 4.0.1. Goldberger-Treiman relations

Partial conservation of axial current (PCAC),  $\partial^\mu A_\mu^a = f_\pi m_\pi^2 \pi^a$ , and the axial Ward Identity,  $\partial^\mu A_\mu^a = 2m_q P^a$ , relate the pion field  $\pi^a$  with the pseudoscalar density:  $\pi^a = (2m_q P^a / f_\pi m_\pi^2)$ , where the pion decay constant  $f_\pi$  is determined from the two-point function  $\langle 0 | A_\mu^a | \pi^b(p) \rangle = i p_\mu \delta^{ab} f_\pi$ .

The renormalized quark mass,  $m_q$ , is given by  $m_q = \frac{m_\pi \langle 0 | \tilde{A}_0^a | \pi^a(0) \rangle}{2 \langle 0 | P^a | \pi^a(0) \rangle}$ , where  $\tilde{A}_0^a$  and  $\tilde{P}^a$  are the renormalized currents. To obtain the  $\pi NN$  and  $\pi N\Delta$  form factors we use the decomposition

$$\begin{aligned} 2m_q \langle N(p') | P^3 | N(p) \rangle &= i \sqrt{\frac{m_N^2}{E_N(\mathbf{p}') E_N(\mathbf{p})}} \frac{f_\pi m_\pi^2 G_{\pi NN}(q^2)}{m_\pi^2 - q^2} \bar{u}(p') \gamma_5 \frac{\tau^3}{2} u(p) \\ 2m_q \langle \Delta(p') | P^3 | N(p) \rangle &= i \sqrt{\frac{2}{3}} \sqrt{\frac{m_\Delta m_N}{E_\Delta(\mathbf{p}') E_N(\mathbf{p})}} \frac{f_\pi m_\pi^2 G_{\pi N\Delta}(q^2)}{m_\pi^2 - q^2} \bar{u}_{\Delta+}^\nu(p') \frac{q_\nu}{2m_N} u_P(p) \end{aligned}$$

PCAC relates the axial form factors  $G_A$  and  $G_p$  with  $G_{\pi NN}$  and equivalently  $C_5^A$  and  $C_6^A$  with  $G_{\pi N\Delta}$ . These are the well known generalized Goldberger-Treiman relations (GTRs). As mentioned above there are advantages in considering ratios. In Fig. 4 we show two such ratios, namely

$G_{\pi N\Delta}/G_{\pi NN}$  and  $2C_5^A/G_A$ . Both are independent of  $Q^2$  and the quark mass. Fitting to a constant we find  $2C_5^A/G_A \sim 1.6 \sim G_{\pi N\Delta}/G_{\pi NN}$ , which implies the Goldberger-Treiman relations:  $G_{\pi NN}(q^2) f_\pi = m_N G_A(q^2)$  and  $G_{\pi N\Delta}(q^2) f_\pi = 2m_N C_5^A(q^2)$ . Assuming pion-pole dominance we can write  $G_p(Q^2) = \frac{4m_N^2/m_\pi^2}{1+Q^2/m_\pi^2} G_A(Q^2)$  and  $C_6^A(Q^2) = \frac{m_N^2/m_\pi^2}{1+Q^2/m_\pi^2} C_5^A(Q^2)$ . Therefore we have the equality  $8C_6^A(Q^2)/G_p(Q^2) = G_{\pi N\Delta}/G_{\pi NN}$ . We find that  $8C_6^A(Q^2)/G_p(Q^2) \sim 1.7$  [13] a few percentage larger than  $G_{\pi N\Delta}/G_{\pi NN}$ .

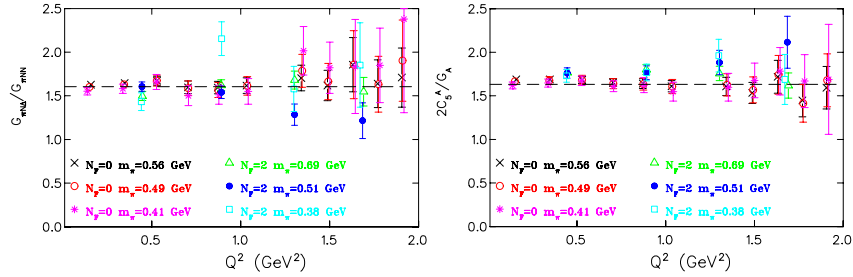


Fig. 4. The ratios  $G_{\pi N\Delta}/G_{\pi NN}$  (left) and  $2C_5^A/G_A$  (right).

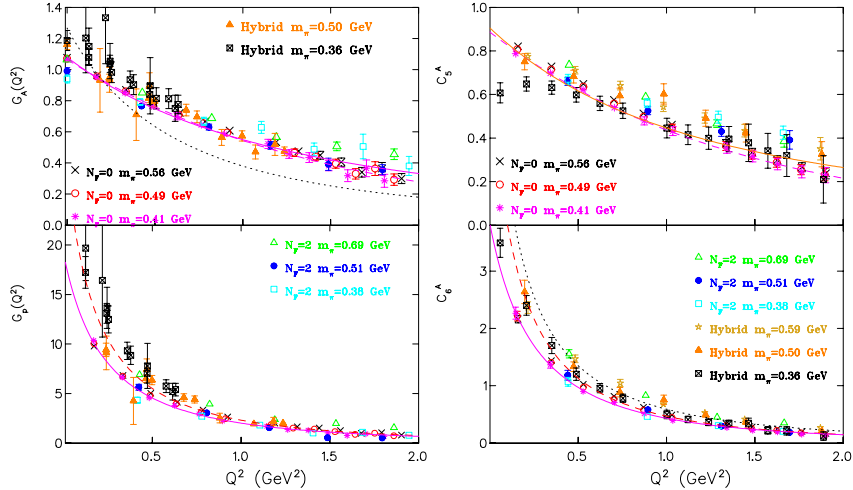


Fig. 5. The nucleon axial form factors  $G_A$  (top, left) and  $G_p$  (bottom, left) and the N to  $\Delta$  axial form factors  $C_5^A$  (top, right) and  $C_6^A$  (bottom, right).

In Fig. 5 we present the nucleon and N to  $\Delta$  axial form factors separately together with fits of  $G_A$  and  $C_5^A$  to a dipole form,  $g_0/(\frac{Q^2}{m_A^2} + 1)^2$ . Dynamical QCD results in the hybrid approach for the smallest pion mass, where we can access low  $Q^2$  values, show large unquenching effects. Having fitted  $G_A$

and  $C_5^A$ , we can check if pion-pole dominance describes the  $Q^2$ -dependence of  $G_p$  and  $C_6^A$ . The dashed lines correspond to the quenched data and show the behavior for  $G_p$  and  $C_6^A$  extracted from fits to  $G_A$  and  $C_5^A$  assuming pion-pole dominance, whereas the dotted line shown for  $C_5^A$  is for the hybrid approach, in both cases for the lightest pion mass. As can be seen, they deviate from the lattice results at low  $Q^2$ . Instead they are best described by the solid curves, which are obtained by fitting the pole mass.

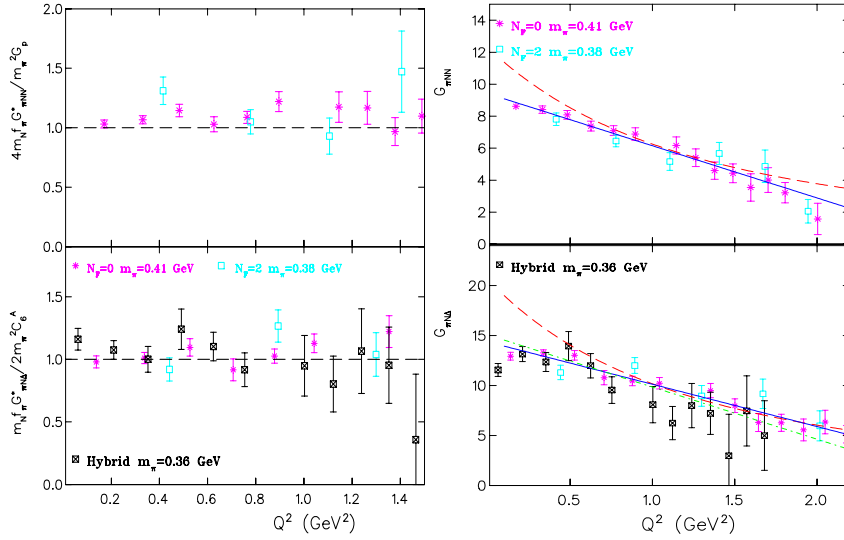


Fig. 6. Left: The ratios  $R_{NN}$  (top) and  $R_{N\Delta}$  (bottom) and right:  $G_{\pi NN}$  (top) and  $G_{\pi N\Delta}$  (bottom) for the smallest pion mass in each type of simulation.

In Fig. 6 we show the relations

$$R_{NN} \equiv \frac{4m_N f_\pi G_{\pi NN}^*(Q^2)}{m_\pi^2 G_p(Q^2)}, \quad R_{N\Delta} \equiv \frac{m_N f_\pi G_{\pi N\Delta}^*(Q^2)}{2m_\pi^2 C_6^A(Q^2)}, \quad (6)$$

where we have defined  $G_{\pi NN}^*(Q^2) \equiv G_{\pi NN}(Q^2)/(1 + Q^2/m_\pi^2)$  with a corresponding expression for  $G_{\pi N\Delta}^*$ . As can be seen these ratios are consistent with unity for all  $Q^2$ -values. Finally, in Fig. 6 we show  $G_{\pi NN}$  and  $G_{\pi N\Delta}$  for the smallest pion mass. The dash lines are obtained from fits of  $G_A$  and  $C_5^A$  via the GTRs,  $G_{\pi NN}(Q^2) = m_N G_A(Q^2)/f_\pi$  and  $G_{\pi N\Delta}(Q^2) = 2m_N C_5^A(Q^2)/f_\pi$ . As can be seen, there are large deviations at small  $Q^2$ . Lattice results at this pion mass give a smaller value in the limit  $Q^2 \rightarrow 0$  than what is extracted from experimental data namely,  $G_{\pi NN}(0) = 13.21(11)$  [14]. The solid lines are fits to the form  $\left(1 - \Delta \frac{Q^2}{m_\pi^2}\right)$

with  $a, \Delta$  fit parameters. Using these fits  $G_{\pi NN}(0)$  and  $G_{\pi N\Delta}(0)$  are extracted (for details see Ref. [13]).

## 5. Conclusions

Lattice results on the electromagnetic, axial-vector and pseudoscalar form factors for the nucleon and the N to  $\Delta$  transition are presented in the quenched approximation, for two-flavors of dynamical Wilson fermions and using dynamical staggered sea quarks and domain wall valence quarks (hybrid approach). Results on the quadrupole to dipole ratios EMR and CMR, obtained in the hybrid approach reaching down to a pion mass of 350 MeV and low  $Q^2$ -values, are non-zero and of similar magnitude as in experiment. We also find that ratios of form factors, such as  $G_{\pi N\Delta}/G_{\pi NN} \sim 1.6$  and  $2C_5^A/G_A \sim 1.6$ , calculated using Wilson fermions, are in agreement with phenomenology. Our results for the ratio  $C_5^A/C_3^V$  as a function of  $Q^2$ , can be regarded as a lattice prediction for the parity violating asymmetry to leading order. The deviations from experiment seen for the magnetic dipole N- $\Delta$  transition form factor  $G_m^*$  and the values of  $G_{\pi NN}$  and  $G_{\pi N\Delta}$  in the limit  $Q^2 \rightarrow 0$  need further study. In particular, finite lattice spacing effects, as well as, chiral extrapolation to the physical pion mass must be investigated.

**Acknowledgments:** I would like to thank my collaborators G. Koutsou, Th. Leontiou, H. Neff, J. W. Negele, W. Schroers and A. Tsapalis for their valuable contributions that made this work possible. This work is supported in part by the EU Integrated Infrastructure Initiative Hadron Physics (I3HP) under contract RII3-CT-2004-506078.

## References

1. C. Mertz *et al.*, *Phys. Rev. Lett.* **86**, 2963 (2001).
2. N. F. Sparveris *et al.*, *Phys. Lett. B* **651**, p. 102 (2007).
3. K. Joo *et al.*, *Phys. Rev. Lett.* **88**, p. 122001 (2002).
4. *PAVI 2002* (unpublished, 2002).
5. K. Orginos, D. Toussaint and R. L. Sugar, *Phys. Rev. D* **60**, p. 054503 (1999).
6. C. Alexandrou *et al.*, *Phys. Rev. Lett.* **94**, p. 021601 (2005).
7. O. Orth, T. Lippert and K. Schilling, *Phys. Rev. D* **72**, p. 014503 (2005).
8. C. Urbach *et al.*, *Comput. Phys. Commun.* **174**, p. 87 (2006).
9. C. N. Papanicolas, *Eur. Phys. J.* **A18**, p. 141 (2003).
10. P. Hägler *et al.*, arxiv:0705.4295.
11. L. Alder, *Ann. Phys.* **50**, p. 189 (1968).
12. N. C. Mukhopadhyay *et al.*, *Nucl. Phys.* **A633**, p. 481 (1998).
13. C. Alexandrou *et al.*, *Phys. Rev. D (in press)*, **arXiv:0706.3011** (2007).
14. H. C. Schröder *et al.*, *Eur. Phys. J.* **C21**, p. 473 (2001).